Variable gas density effects on transport from interacting evaporating spherical drops

G.E. Cossali and S. Tonini

May 29, 2018

Abstract

The paper reports an analytical approach to model heat and mass transfer from neighbouring spherical drops accounting for the dependence of the gas mixture density on temperature and composition. The conservation equations for single-component non-identical spherical drops evaporating in gaseous quiescent environment are analytically solved in a bi-spherical coordinate system. Analytical expressions for the local heat and mass fluxes on drop surfaces and for the evaporation and the sensible heat rates are reported. The effect of relieving the commonly adopted assumption of constant gas density is quantified by comparison with existing constant density solutions for different evaporating species and operating conditions. The model applies to any value of Lewis number. Comparison with analogous results for single isolated drops allows to quantify the screening effect on vapour and heat fluxes and evaporation and heat rates.

1 Nomenclature

a	length scale in bi-spherical coordinates	m
A	drop surface area	m^2
b_p	series coefficients, Eq. (22)	-
c	molar density	$kmol\ m^{-3}$
$c_{p,v}$	vapour specific heat capacity	$J\ kg^{-1}K^{-1}$
D_{10}	binary diffusion coefficient	m^2s^{-1}
D_{av}	average drop diameter	m
Ec	Eckert number, $Ec = \frac{\lvert U\rvert^2}{c_{p,v}(T_\infty - T_s)}$	-
F	auxiliary harmonic function	-
g_p	series coefficients, Eq. (22)	-
h_η, h_ξ, h_φ	scale factors for η, ξ and φ coordinates	m
H	non-dimensional function, $H = \ln\left(1 - y^{(0)}\right)$	-
k	thermal conductivity	$W\ m^{-1}K^{-1}$
L	drop distance, $L = z_1 - z_2$, Figure 1.	m
Le^M	modified Lewis number, $Le^M = \frac{k}{c_{p,v}\ D_{10} M_m^{(1)} c_{ref}}$	-
m_{ev}	evaporation rate	$kg\ s^{-1}$
$m_{ev,is}$	evaporation rate from an isolated drop	$kg\ s^{-1}$
M_m	molar mass	$kg\ kmol^{-1}$
$M_0,\ M_0^c$	model constants	-
n	mass flux	$kg\ m^{-2}s^{-1}$
N	molar flux	$kmol\ m^{-2}s^{-1}$
P_n	Legendre polynomials	-
P_T	gas pressure	Pa
q	heat flux	$W\ m^{-2}$
Q	heat rate	W
$\bar{R}$	universal gas constant	$J\ kmol^{-1}\ K^{-1}$
R_d	drop radius	m
Sc^M	modified Schmidt number, $Sc^M = \frac{\mu}{D_{10}\ c_{ref}\ M_m^{(1)}}$	-
T	temperature	K

U	Stefan velocity	$m\ s^{-1}$
x, y, z	Cartesian coordinates	m
$y^{(p)}$	molar fraction of p-component	-
$\delta n\%$	non-uniformity parameter, Eq. (48)	-
$\Delta n_{\max}\%$	shield parameter, Eq. (49)	-

Greek symbols

α_{ref}	averaging parameter, Eq. (11)	-
β	distance parameter	-
δ	drop radii ratio, $\delta = \frac{R_{d,2}}{R_{d,1}}$	-
η, ξ, φ	bi-spherical coordinates	-
θ	zenital angle	deg
μ	shear viscosity	$kg\ \ m^{-1}\ s^{-1}$
ρ	mass density	$kg\ m^{-3}$
ϕ	screening coefficient	-
χ	mass fraction	-
Λ	non-dimensional parameter, $\Lambda = \frac{\bar{R}T_\infty R_d^2}{M_m^{(1)} D_{10}^2}$	-
Φ	non-dimensional function, $\Phi = \cosh\eta - \cos\xi$	-

Subscripts

ad non-dimensional

b drop number

c constant density model

is isolated drop

ref reference conditions

s drop surface

v vapour

th thermal

∞ ambient conditions

Superscripts

0 non-vaporising species

1 vaporising species

$\sim$ non-dimensional

c constant density model

T total

Abbreviation

B.C. Boundary Condition

CFD Computational Fluid Dynamics

CPU Central Processing Unit

DNS Direct Numerical Simulation

LHS Left Hand Side

PDE Partial Differential Equation

2 Introduction

Spray drop evaporation is a key phenomenon in many industrial applications and in many fields, like automotive, aeronautics, fire suppression, painting, medical aerosol, etc. Modelling of spray evaporation relies on single drop

evaporation models and an extensive literature on this subject is available (see [1] and [2] for a recent literature review), although some of the mechanisms governing the phase transition and mass/energy transport within the gas and liquid phases are currently not yet fully understood [3]. Analytical models of single drop heating and evaporation (among which [4] is the most widespread) are at present implemented in most of the commercial CFD codes used to investigate the behaviour of complex multi-drop systems. An extensive work is underway to develop new analytical models to cope with the double aim to relieve some stringent assumptions, present in most of the existing approaches, and to produce more CPU efficient models [2]. However, the implemented models are derived and validated for single drop heating and evaporation, therefore they cannot fully account for the effect of drop neighbouring. The need of sound predictive tools of heating and evaporation of drops in the dense spray region is widely recognised and reliable predictions under those conditions, where drop-to-drop interactions play a dominant role, are considered essential, for example to optimise the design of combustion chambers [5].

One of the first experimental studies on the effect of drop interaction on the ignition time was reported in [6] for a drop stream injected into a hot gas; the study evidenced that a closer spacing between drops noticeably influences heat and mass diffusion from the flame region. Further experimental work on drop lifetime led to the conclusion [7] that the classical "D^2-Law", widely used to account for time dependent evaporation of a single drop, may not be strictly applicable to interacting drops.

The evaporation of mono-sized periodically arranged drops were the subject of more recent experimental studies [8], [9], and the results suggest that the evaporation rate is significantly reduced when the distance parameter (the drop spacing non-dimensionalised by the drop diameter) becomes smaller than 8. In [9] and [10] a correlation was separately proposed, to correct the Sherwood and Nusselt numbers of the isolated drop by a coefficient depending on the distance parameter. More recently, the heating and evaporation rates of drop chains made of different species (n-dodecane, n-decane, iso-hexane and ethanol) [5] were measured, with the aim of extending previous experimental works on the evaporation of interacting drops [11], [12], [13]; the Authors concluded that the drop spacing heavily influences the development of a boundary layer around the chain of drops and consequently affects drop size and temperature evolutions.

Modelling of the heating and evaporation of mutually interacting drops were mainly considered in the field of combustion and theoretical and numerical investigations are reported by various researchers.

On the numerical side, a relevant amount of work can be found in the literature, starting from [14], [15] where the interaction of two and three evaporating drops was numerically simulated, accounting for the effect of the drop motion, variable thermo-physical properties, transient heating and internal circulation in the liquid phase, boundary-layer blowing and moving interface due to surface regression (see [16], for a recent review). Numerical study on the vaporization of three-dimensional drop arrays were considered for example in [17], and [18] with the main aim to correlate the burning rates with the number of drops, the average drop size and the average spacing. DNS was performed for a drop stream in [19], taking into account the effect of non-uniform and transient stress at drop surface. Numerical simulation of evaporation in a monodisperse drop stream was proposed by [20], focusing on the drop internal motion driven by viscous and Marangoni forces.

An analytical approach to the problem was first proposed by [21], which solved the conservation equations in a bi-spherical coordinate system, for the case of negligible Stefan flow. The effect of non-negligible Stefan flow was then introduced by [22], which analysed the effect of drop spacing on evaporation in regular arrays (triangular and tetrahedral). Analytical solutions in bi-spherical coordinates were then proposed, for identical and non-identical couples of drops, by [23], [24], for unitary Lewis number. The general theory proposed by [22] was then used by many Authors to study more complex clusters of drops, in combusting environment [25] or for clusters of up to 100 randomly spaced drops [26]. A generalised approach to treat vaporization in dense drop arrays was proposed in [27]. Most of the studies were limited to unitary values of the Lewis number and an extension of the analysis to the case of non-unitary Lewis number was first proposed in [28]. All the *available analytical solutions* rely on the assumption of constant properties of the gaseous mixture and they need to define reference values, and a proper procedure to evaluate average transport properties was proposed in [18].

As a first attempt to relieve the assumption of constant gas mixture properties, the present paper reports an exact analytical solution of the problem of heat and mass transfer from a couple of spherical single-component non identical drops evaporating in a stagnant environment, accounting for the dependence of the gas mixture density on temperature and composition and for any value of the Lewis number.

The following sections reports the mathematical description of the model, the application to four different evaporating species at different operating conditions and a comparison with existing solutions for the case of constant gas density.

3 Mathematical model

The model described below retains some important approximations that characterise the analytic approach to model heating and evaporation of two liquid drops, like sphericity of each drop and quasi-steadiness, among others, while relieving an important limitation, namely the constancy of the gas density. The steady-state energy, momentum and species conservation equations will be written and analytical solutions will be presented by using bi-spherical coordinates. To model the evaporation of single component drops under quasi-steady conditions the following species conservation equations are needed:

$$\nabla_j N_j^{(p)} = 0 \qquad p = (0,1) \tag{1}$$

where

$$N_j^{(p)} = N_j^{(T)} y^{(p)} - cD_{10} \nabla_j y^{(p)} \tag{2}$$

are the molar fluxes, and $p = 0, 1$ stand for the non-evaporating *(gas)* and evaporating *(vapour)* species, respectively, $N_j^{(T)} = N_j^{(0)} + N_j^{(1)}$, $y^{(p)}$ is the molar fraction of the species p and c is the molar gas density that, under the assumption of ideal behaviour of the gaseous mixture, can be evaluated as:

$$c = \frac{P_T}{\bar{R}T} \tag{3}$$

The usual way to approach this problem is by using a mass form of the species conservation equations (see [4], [29]), but it can be shown (see [30]) that, for single component drops, the two approaches are equivalent, and mass fluxes can be obtained by $n_j^{(p)} = N_j^{(p)} M_m^{(p)}$. The mass density depends also on composition, since for an ideal binary mixture:

$$\rho = \frac{P_T M_m^{(0)}}{\bar{R}T} \left(1 + \frac{M_m^{(1)} - M_m^{(0)}}{M_m^{(0)}} y^{(1)} \right) \tag{4}$$

using the molar approach, where the molar density c depends only on temperature and pressure, simpler forms of the final solutions are obtained.

Assuming stationary liquid-gas interface and absence of diffusion of the component $p = 0$ into the liquid drop (i.e. pure liquid) yields a nil flux of this component everywhere, and the first of equations (2) yields:

$$N_j^T = cD_{10} \nabla_j H \tag{5}$$

where $H = \ln y^{(0)}$.

Summation of equations (1) yields the mass conservation equation:

$$\nabla_j \left(\rho U_j\right) = 0 \tag{6}$$

and, since under the mentioned assumptions: $\rho U_j = n_j^T = n_j^{(1)} = M_m^{(1)} N_j^T$, equations (6) and (5) yield:

$$\nabla_j \left(c \nabla_j H\right) = 0 \tag{7}$$

To notice that, since equations (1), (2) and (6) are not independent, one of the species conservation equations can be disregarded.

The sensible heat exchanged by the evaporating drop can be quantified by solving the energy equation*, assuming constant conductivity* k *and vapour specific heat capacity* $c_{p,v}$*,* (see also [30]):

$$\rho U_j \nabla_j T = \frac{k}{c_{p,v}} \nabla^2 T \tag{8}$$

where dissipation by viscous stress is neglected since the Eckert number $Ec = \frac{|U|^2}{c_{p,v}(T_\infty - T_s)}$ *is very small, particularly in case of large temperature difference. Inter-diffusional terms are accounted for as in [31], while further minor terms (refer to [32], p. 589, or [33] p. 465 for the complete equation) are neglected.*

Using equation (7) and (5), equation (8) can be written as:

$$M_m^{(1)} c D_{10} \nabla_j H \nabla_j T = \frac{k}{c_{p,v}} \nabla^2 T \tag{9}$$

The momentum conservation equation for the evaporating drop, under the same simplifying hypotheses and assuming constant shear viscosity and neglectful bulk viscosity, as in [34], is:

$$\rho U_j \nabla_j U_k = -\nabla_k P_T + \mu \nabla^2 U_k \tag{10}$$

Equations (7), (9) and (10) are rather general and they can be used to model the evaporation from any shape and position of the evaporating surfaces, since these information enter the problem only through the boundary conditions. To allow a simpler approach, these equations are non-dimensionalised introducing the non-dimensional velocity ($\tilde{U} = U \frac{R_d}{D_{10}}$) and pressure ($\tilde{P}_T = \frac{P_T}{c_{ref} \bar{R} T_\infty}$), modified Schmidt number ($Sc^M = \frac{\mu}{D_{10}\ c_{ref}\ M_m^{(1)}}$), modified Lewis number ($Le^M = \frac{k}{c_{p,v}\ D_{10} M_m^{(1)} c_{ref}}$) and the parameter $\Lambda = \frac{\bar{R} T_\infty R_d^2}{M_m^{(1)} D_{10}^2}$; the non-dimensional nabla operator $\hat{\nabla}_j = R_d \nabla_j$ will be written omitting the hat symbol.

In the proposed model $c_{p,v}$, D_{10}, μ and k are assumed to be constant and evaluated at some reference conditions, which are usually defined as:

$$T_{ref} = \alpha_{ref} T_\infty + (1 - \alpha_{ref})\, T_s; \quad \chi^{(1)}_{ref} = \alpha_{ref} \chi^{(1)}_\infty + (1 - \alpha_{ref})\, \chi^{(1)}_s \tag{11}$$

where $\chi^{(1)}$ is the mass fraction of the evaporating species. The classical value for α_{ref} is 1/2, but often the value $\alpha_{ref} = 1/3$, suggested in [35] (the so-called "$1/3^{rd}$ rule") is used, as in [4] for example and in the present investigation.

Equations (7), (9) and (10) then become:

$$\nabla_j \left(\tilde{P}_T \tilde{T}^{-1} \nabla_j H \right) = 0 \tag{12}$$

$$\tilde{P}_T \tilde{T}^{-1} \nabla_j H \nabla_j \tilde{T} = Le^M \nabla^2 \tilde{T} \tag{13}$$

$$\nabla_k \tilde{P}_T = \frac{1}{\Lambda} \left[Sc^M \nabla^2 \tilde{U}_k - \tilde{P}_T \tilde{T}^{-1} \nabla_j H \nabla_j \tilde{U}_k \right] \tag{14}$$

where $\tilde{T} = \frac{T}{T_\infty}$. It has already been shown, [34] and [36], that for a large variety of conditions of interest for applications, the non-dimensional parameter Λ assumes quite large values, then justifying the use of an asymptotic form (for $\Lambda \to \infty$) of the momentum equation, that in the present case yields: $\nabla_k \tilde{P}_T = 0$ and then $\tilde{P}_T = const.$ Since in this case: $P_T = P_{T,\infty}$, under the assumption of ideal gas behaviour for the gaseous mixture, and defining $\tilde{c} = \frac{c}{c_{ref}}$, equation (3) yields:

$$\tilde{c}\tilde{T} = \check{P}_{T,\infty} = \frac{c_\infty}{c_{ref}} = \frac{T_{ref}}{T_\infty} = \tilde{T}_{ref} \tag{15}$$

and equations (12) (13) *yield the following system of non-linear PDEs*:

$$\nabla_j \left(\tilde{T}^{-1} \nabla_j H \right) = 0 \tag{16}$$

$$\frac{\tilde{T}_{ref}}{Le^M} \left(\tilde{T}^{-1} \nabla_j H \right) \nabla_j \tilde{T} = \nabla^2 \tilde{T} \tag{17}$$

3.1 Solution in a bi-spherical coordinate system

In the present investigation the evaporation of two drops of any radius positioned at any distance from each other, larger than the sum of the two drop radii to avoid interference (see figure 1), will be investigated by solving analytically equations (16, 17) with uniform Dirichlet conditions on drop surfaces. To this end, bi-spherical coordinates will be

used and their definition is given by the equations (see also [37]):

$$x = a\frac{\sin\xi\sin\phi}{\Phi};\quad y = a\frac{\sin\xi\cos\phi}{\Phi};\quad z = a\frac{\sinh\eta}{\Phi}; \tag{18}$$

$$\Phi = \cosh\eta - \cos\xi \tag{19}$$

and represented graphically in figure 2; the surface $\eta = \eta_0$ is a sphere with radius $R_d = \frac{a}{|\sinh\eta_0|}$ centered in $z_0 = a\coth\eta_0$, the surface $\xi = \xi_0$ is generated by the rotation of an arc of a circumference around the z-axis and it can be seen as self-intersecting torus. The surface $\varphi = \varphi_0$ is a plane passing through the z-axis.

Considering this coordinate system, and referring to figure 1, the sphere centered on the z-axis in $z = z_1$ has equation $\eta = \eta_1$, while the one centered in $z = z_2$ has equation $\eta = \eta_2$. The radii of the spheres and the drop distance define the parameters a, η_1 η_2 through the equations:

$$\begin{aligned} R_{d,1} &= \frac{a}{\sinh\eta_1};\ R_{d,2} = \frac{a}{|\sinh\eta_2|} \\ L &= z_1 - z_2 = a\left(\coth\eta_1 - \coth\eta_2\right) \end{aligned} \tag{20}$$

where $\eta_1 > 0$ and $\eta_2 < 0$ and $z_1 = a\coth\eta_1;\ z_2 = a\coth\eta_2$.

Consider an auxiliary function F, harmonic (i.e. $\nabla^2 F = 0$) and symmetric around the z-axis, equal to 1 over the surface of the two drops and nil at infinity. Since in bi-spherical coordinates the Laplace equation is:

$$\frac{\partial}{\partial\eta}\left(\frac{\sin\xi}{\Phi}\frac{\partial F}{\partial\eta}\right) + \frac{\partial}{\partial\xi}\left(\frac{\sin\xi}{\Phi}\frac{\partial F}{\partial\xi}\right) = 0 \tag{21}$$

the function F has the the explicit form:

$$F = \Phi^{1/2}\sum_{p=0}^{\infty} P_p\left(y\right)\left\{g_p\cosh\left(p+\frac{1}{2}\right)\eta + b_p\sinh\left(p+\frac{1}{2}\right)\eta\right\} \tag{22}$$

where $y = \cos\xi$ and $P_p\left(y\right)$ is the Legendre polynomial of degree p *(see [37] for further details).*

It can be easily shown that the function F, defined by equation (22), satisfies the condition at infinity and the following choice of the coefficients g_p, b_p:

$$g_p = \sqrt{2}\frac{\left[\sinh\left[\left(p+\frac{1}{2}\right)\eta_2\right]e^{-\left(p+\frac{1}{2}\right)\eta_1} - \sinh\left[\left(p+\frac{1}{2}\right)\eta_1\right]e^{\left(p+\frac{1}{2}\right)\eta_2}\right]}{\sinh\left[\left(p+\frac{1}{2}\right)\left(\eta_2-\eta_1\right)\right]}; \tag{23}$$

$$b_p = \sqrt{2}\frac{\left[\cosh\left[\left(p+\frac{1}{2}\right)\eta_2\right]e^{-\left(p+\frac{1}{2}\right)\eta_1} - \cosh\left[\left(p+\frac{1}{2}\right)\eta_1\right]e^{\left(p+\frac{1}{2}\right)\eta_2}\right]}{\sinh\left[\left(p+\frac{1}{2}\right)\left(\eta_1-\eta_2\right)\right]} \tag{24}$$

where the following identity (see [38]):

$$\frac{1}{\Phi^{1/2}} = \sqrt{2}\sum_{p=0}^{\infty} P_p\left(y\right) e^{-(p+1/2)|\eta|} \tag{25}$$

was used, ensures that $F\left(\eta_1, \xi\right) = F\left(\eta_2, \xi\right) = 1$.

The solution of equations (16, 17) with B.C.:

$$\begin{aligned} \tilde{T} &= \tilde{T}_s;\ H = H_s \text{ on the surfaces} \\ \tilde{T} &= 1;\ \ H = H_\infty \text{ at infinity} \end{aligned}$$

is then given by:

$$\tilde{T} = \frac{1 - e^{M_0 F}}{1 - e^{M_0}}\left(\tilde{T}_s - 1\right) + 1 \tag{26}$$

$$H - H_\infty = \frac{Le_M}{\tilde{T}_{ref}}\left[\frac{\tilde{T}_s - 1}{1 - e^{M_0}}\left(1 - e^{M_0 F}\right) + \frac{\tilde{T}_s - e^{M_0}}{1 - e^{M_0}} M_0 F\right] \tag{27}$$

where the constant M_0 is obtained by solving the equation:

$$H_s - H_\infty = \frac{Le^M}{\tilde{T}_{ref}}\left[\tilde{T}_s - 1 + \frac{\tilde{T}_s - e^{M_0}}{1 - e^{M_0}} M_0\right] \tag{28}$$

as it can be proven by direct substitution. *To be noticed that H_s is a function of the surface drop temperature since the vapour molar fraction is taken at its saturation value for that temperature.*

Without loss of generality, the drop number 2 will always be the smaller one and always centered in $z_2 < 0$, thus the drop radii ratio defined by:

$$\delta = \frac{R_{d,2}}{R_{d,1}} \tag{29}$$

will always be lower than or equal to 1. The definition of a non-dimensional distance parameter [1] in this case is not univocal. The following definition will be assumed:

$$\beta = \frac{L}{D_{av}} = \frac{z_1 - z_2}{D_{av}} \tag{30}$$

where D_{av} is a reference drop diameter defined as $D_{av} = R_{d,1} + R_{d,2}$; in this way the usual definition is recovered when the two drops are identical.

3.1.1 The constant gas density case

The solutions above described can be compared to those obtained when the gas density is assumed constant, in that case equations (7) and (9) become:

$$\begin{aligned} \nabla^2 H &= 0 \\ \frac{1}{Le^M}\nabla_j H \nabla_j \tilde{T} &= \nabla^2 \tilde{T} \end{aligned}$$

and the solutions are:

$$H = H_\infty + (H_s - H_\infty) F \tag{31}$$

$$\tilde{T} = \frac{1 - e^{M_0^c F}}{1 - e^{M_0^c}} \left(\tilde{T}_s - 1\right) + 1 \tag{32}$$

with: $M_0^c = \frac{(H_s - H_\infty)}{Le^M}$. This derivation, in a different form, can also be found *for example* in [24].

Interestingly, the solution for the vapour distribution can be extended also to the case when the two drop surfaces are at different temperature, by defining:

$$H = \Phi^{1/2} \sum_{p=0}^{\infty} P_p(y) \left\{ g_p \cosh\left(p + \frac{1}{2}\right)\eta + b_p \sinh\left(p + \frac{1}{2}\right)\eta \right\} \tag{33}$$

where

$$g_p = \sqrt{2} \frac{\left[\begin{array}{l} H_{s1} \sinh\left[\left(p + \frac{1}{2}\right)\eta_2\right] e^{-\left(p+\frac{1}{2}\right)\eta_1} \\ -H_{s2} \left[\sinh\left(p + \frac{1}{2}\right)\eta_1\right] e^{\left(p+\frac{1}{2}\right)\eta_2} \end{array} \right]}{\sinh\left[\left(p + \frac{1}{2}\right)(\eta_2 - \eta_1)\right]}; \quad b_p = \sqrt{2} \frac{\left[\begin{array}{l} H_{s1} \left[\cosh\left(p + \frac{1}{2}\right)\eta_2\right] e^{-\left(p+\frac{1}{2}\right)\eta_1} \\ -H_{s2} \cosh\left[\left(p + \frac{1}{2}\right)\eta_1\right] e^{\left(p+\frac{1}{2}\right)\eta_2} \end{array} \right]}{\sinh\left[\left(p + \frac{1}{2}\right)(\eta_1 - \eta_2)\right]}$$

then equation (33) satisfies the B.C.

$$H(\eta_1, \xi) = H_{s1}; \; H(\eta_2, \xi) = H_{s2} \tag{34}$$

However, it should be noticed that for the case of drops at different temperatures ($H_{s1} \neq H_{s2}$), to the best knowledge of the Authors, no analytical solution is at present available for the energy equation.

Figure 3 reports the distribution of the vapour mass fractions, in terms of $H = \ln\left(1 - y^{(1)}\right)$, for two identical (figure 3a) and non-identical (figure 3b) water drops, comparing the results with those obtained assuming constant gas density. The effect is evident, but its intensity depends, as expected, by the species properties and the next section reports a comparison for different species.

3.2 Application to different vaporising species

Four different species were considered, namely water, n-octane, n-dodecane and acetone. The first three species were chosen since their properties are characteristics of fluids used in practical applications (fire control, gasoline and diesel engines), acetone was chosen for its high volatility. Two identical drops are considered here, with radius equal to $20\mu m$ and $\beta = 2$. *Under the selected operating conditions, the parameter* Λ *in the momentum equation (14) ranges from* $3.0 \cdot 10^4$ *for the case of water drop evaporating in air at 1000K up to* $1.2 \cdot 10^5$ *for acetone drop in air at 500K, confirming that the assumption of constant pressure is applicable.*

The effect of different drop size and inter-axial distance will be analysed below. To yield a comparison that may be linked to applicative conditions, the drop temperatures were chosen to be equal to the plateau temperature reached by a single drop while it is vaporising under the same conditions (refer to Table 1); these plateau temperatures were estimated by a heat and mass balance performed by using the model proposed in [36], where, as in the present case, the gas density was assumed to depend on gas temperature and composition.

Figure 4 reports the profiles of the vapour molar fraction, always in terms of $H = \ln\left(1 - y^{(1)}\right)$, along the z-coordinate (see figure 1), for the twelve test cases reported in Table 1, comparing the solutions for the variable gas density (Eq. 27) and the constant gas density (Eq. 33) models. The assumption of constant gas density leads to an underestimation of the vapour molar fraction distribution. The increase of the gas temperature, and the consequent increase of the drop temperature, enhances the differences between the two models. The largest effect is seen for the most volatile species (acetone), while with n-dodecane, the less volatile and with the highest molar mass, the differences between the two models are the smallest and become almost negligible for the lowest gas temperature (500K).

Figure 5 reports the corresponding profiles of the vapour molar fraction ($H = \ln\left(1 - y^{(1)}\right)$) along the r-coordinate starting from the centre of each drop, for the same species and conditions of figure 4, confirming the above described trends.

The next section reports the evaluation of the heat and mass fluxes that can be obtained from the above reported analytical solutions and the corresponding heat and evaporation rates.

Table 1. Drop surface temperature for the cases reported in figures 4 and 5.

Species	$T_\infty = 500$ K	$T_\infty = 750$ K	$T_\infty = 1000$ K
water	$317.1K$	$331.6K$	$339.5K$
acetone	$291.8K$	$302.8K$	$308.5K$
n-octane	$351.4K$	$366.1K$	$372.7K$
n-dodecane	$418.7K$	$443.6K$	$452.5K$

4 The local and global heat and evaporation rates

The vapour mass flux component normal to the drop surfaces can be evaluated, considering that the coordinate η is normal to the sphere $\eta = const$, from Eqs. (2), (27):

$$n_1^{(1)} = -M_m^{(1)} c_{ref} D_{10} Le^M M_0 \left(\frac{1}{h_\eta}\frac{\partial F}{\partial \eta}\right)_{\eta=\eta_1} \tag{35}$$

$$n_2^{(1)} = M_m^{(1)} c_{ref} D_{10} Le^M M_0 \left(\frac{1}{h_\eta}\frac{\partial F}{\partial \eta}\right)_{\eta=\eta_2} \tag{36}$$

where the minus sign comes from the fact that η goes to infinity towards the inner part of the drop-1, while the opposite happens for drop-2, and the scaling function along η is:

$$h_\eta = \frac{a}{\Phi} \tag{37}$$

The total evaporation rate can be found integrating the vapour mass flux over the drops surface, then:

$$m_{ev,(b)} = \int_{A_1} n_{(b)}^{(1)} dA = (-1)^{b+1} \int_0^{2\pi}\int_0^{\pi} M_m^{(1)} c_{ref} D_{10} Le^M M_0 \left(\frac{1}{h_\eta}\frac{\partial F}{\partial \eta}\right)_{\eta=\eta_{(b)}} h_\xi h_\varphi d\xi d\varphi \tag{38}$$

where b=1,2, and

$$h_\xi = \frac{a}{\Phi}; \quad h_\varphi = a\frac{\sin\xi}{\Phi} \tag{39}$$

are the scaling functions of the ξ and φ coordinates, respectively.

An analytical solution of the integrals (38) can be calculated and, using some properties of Legendre polynomials,

the following closed forms can be obtained:

$$m_{ev,1} = -2\sqrt{2}\pi a M_m^{(1)} c_{ref} D_{10} L e^M M_0 \sum_{p=0}^{\infty} (g_p + b_p) \tag{40}$$

$$m_{ev,2} = -2\sqrt{2}\pi a M_m^{(1)} c_{ref} D_{10} L e^M M_0 \sum_{p=0}^{\infty} (g_p - b_p) \tag{41}$$

The parameter a, appearing in the above equations, can be explicitly evaluated as a function of the drop radii and their distance from equation (20) yielding:

$$a = \frac{R_{d,1}}{2} \left\{ \beta^2 (1+\delta)^2 - 2\left(1+\delta^2\right) + \frac{\left(1-\delta^2\right)^2}{(1+\delta)^2 \beta^2} \right\}^{1/2} \tag{42}$$

To notice that for the case of two identical drops $\eta_2 = -\eta_1$ the coefficients b_p are all nil and

$$g_p = \sqrt{2} \frac{2\sinh\left[\left(p+\frac{1}{2}\right)\eta_1\right]}{\sinh\left[2\left(p+\frac{1}{2}\right)\eta_1\right]} e^{-\left(p+\frac{1}{2}\right)\eta_1} \tag{43}$$

Equations (40) and (41) resemble equations (15) in [24], with the difference that the presence of the parameter M_0, which depends form the boundary and operating conditions (Eq. 28) allows to account for the effect of gas density dependence on temperature and composition.

The heat flux component normal to the drop surfaces can be evaluated as:

$$q_{(b)} = (-1)^{b+1} k \frac{1}{h_\eta} \left(\frac{\partial T}{\partial \eta} \right)_{\eta=\eta_{(b)}} = \left(\tilde{T}_s - 1 \right) \frac{e^{M_0}}{\left(1 - e^{M_0}\right)} c_{p,v} n_{(b)}^{(1)} \tag{44}$$

where Eqs. (35), (36) and (26) were used. The heat fluxes are then directly proportional to the corresponding vapour fluxes and their explicit forms can be calculated from Eqs. (35), (36).

The heat rate can be calculated by integrating the heat flux over the drop surface yielding:

$$Q_{(b)} = \int_{A_{(b)}} q_{(b)} dA = \left(\tilde{T}_s - 1 \right) \frac{e^{M_0}}{\left(1 - e^{M_0}\right)} c_{p,v} \int_{A_{(b)}} n_{(b)}^{(1)} dA = \left(\tilde{T}_s - 1 \right) \frac{e^{M_0}}{\left(1 - e^{M_0}\right)} c_{p,v} m_{ev,(b)}$$

Applying the same procedure to equations describing the constant density model (Eqs. 31 and 32), yields the same results for the heat fluxes ($q_{(b),c}$) and vapour fluxes ($n_{(b),c}^{(1)}$), where the constant M_0 (calculated by Eq. 28) is replaced by $M_0^c = \frac{(H_s - H_\infty)}{L e^M}$.

The next section reports an application of these results to different vaporising species.

4.1 Vapour fluxes distributions for different vaporising species

The model was applied to evaluate the vapour flux on the two drop surfaces, for the cases reported in table 1.

The heat and vapour fluxes over one drop surface depend on the position due to the screening effect of the neighbouring drop, and they can be compared to the corresponding (uniform) fluxes over the surface of an isolated spherical drop.

The evaporation rate of an isolated drop can be calculated, accounting for a non constant gas density, using Eqs. (18) and (19) of [30], yielding:

$$m_{ev,is} = -4\pi R_j M_m^{(1)} c_{ref} D_{10} Le^M Y$$

where Y is found from:

$$\left[\frac{T_s - e^{-Y}}{1 - e^{-Y}} Y + (1 - T_s)\right] = \tilde{T}_{ref} \frac{1}{Le^M} (H_s - H_\infty) \tag{45}$$

and a comparison of (28) with (45) shows that $Y = -M_0$. The corresponding vapour flux is then:

$$n_{is}^{(1)} = M_m^{(1)} c_{ref} D_{10} Le^M \frac{M_0}{R_d} \tag{46}$$

and using this to non-dimensionalise the vapour flux from the interacting drop yields:

$$n_{ad,(b)} = \frac{n_{(b)}^{(1)}}{n_{is}^{(1)}} = (-1)^{b+1} \left(\frac{R_d}{h_\eta} \frac{\partial F}{\partial \eta}\right)_{\eta=\eta_{(b)}} \tag{47}$$

showing that the non-dimensional flux distribution is independent of the species and operating conditions. Making use of Eqs. (42) and (37), it is easy to see that $n_{ad,(b)}$ depends only on δ, β and the position on the drop surface.

The profile of the non-dimensional vapour mass flux is then reported, as function of the angle θ (refer to figure 1), for the case of two identical drops ($\delta = 1$) and for different values of β, in figure 6(a). The maximum of the surface vapour flux is clearly found on the location farthest form the other drop ($\theta = 0$ deg), and the screening effect of the other drop is the cause of the flux decrease while moving towards the opposite side ($\theta = 180$ deg). As expected, the increase of β diminishes the interaction and the flux distributions tend to that of an isolated drop. The non-uniformity of the vapour flux along the drop surface can be measured as the relative difference between the maximum and minimum values:

$$\delta n \ \% = \frac{n_{ad,(1),\max} - n_{ad,(1),\min}}{n_{ad,(1),\max}} \times 100 \tag{48}$$

and it is reported as function of β in figure 6(b). With the increase of β, the flux non-uniformity diminishes and the maximum non-dimensional vapour flux ($n_{ad,(1),\max}$) must approach 1, since the screening effect of the other drop vanishes. However, the reported results shows that the effect of screening on the flux non-uniformity vanishes much

faster than the effect on the maximum value. The second curve in figure 6(b) reports the values of:

$$\Delta n_{\max}\ \% = \left(1 - n_{ad,(1),\max}\right) \times 100 \tag{49}$$

and it can be seen that when δn % reaches 0.1% (vanishing of flux non-uniformity), the value of $\Delta n_{\max}$ % is still more than 10 times (1.2%).

Figure 6(a) also shows the vapour mass flux calculated assuming constant density, non-dimensionalised again by the same vapour flux from an isolated drop, Eq. (46):

$$n^c_{ad,(b)} = \frac{n^{(1)}_{(b),c}}{n^{(1)}_{is}} = n_{ad,(b)} \frac{M^c_0}{M_0}$$

and the substitution of: $(H_s - H_\infty) = M^c_0 L e^M$ (from the definition of M^c_0) into the LHS of Eq. (28) shows that the ratio $\frac{M^c_0}{M_0}$ depends on the operating conditions through $\tilde{T_s}$ and M^c_0, as reported in figure 7. The constant density model predicts larger values of vapour flux. The differences between the two models are found to depend on the operating conditions and evaporating species. Figure 8 shows non-dimensional vapour fluxes for the conditions reported in table 1. The black curve refers to the variable density model (a single curve since $n_{ad,(b)}$ is independent on species and operating conditions), while the other curves report the profiles of the non-dimensional vapour flux predicted by the constant density model for the four selected species and the three gas temperatures. It can be noticed that the reported dependence on the gas temperature may be non-monotonic (acetone, n-octane and n-dodecane). This behaviour comes from the choice of using, for each species, the plateau temperature, which depends on the gas temperature, as above reported. Figure 7 shows the values (symbols) of the ratio $\frac{M^c_0}{M_0}$ for the cases of table 1, confirming that the non-monotonic behaviour is due to the choice of the drop temperature. The curve joining the symbols corresponding to n-dodecane was obtaining evaluating the plateau temperature for different gas temperatures to enlighten the non-monotonic behaviour. *Recalling the definition of the reference temperature (11) and equation (28), the value of the averaging parameter α_{ref} that would yield $\frac{M^c_0}{M_0} = 1$, assuring that the constant density model predicts the same result that the variable density one, would be:*

$$\alpha_{ref} = -\left(\frac{1}{M^c_0} + \frac{e^{M^c_0}}{1 - e^{M^c_0}}\right)$$

This fact was already observed in [30] for the case of a single spherical drop. It is clear that the value of α_{ref} that would satisfy this requirement depends on the evaporation rate (through M_0), and, as already reported in [30],

the choice $\alpha_{ref} = 1/2$ fits well for very low values of the evaporation rate, while $\alpha_{ref} = 1/3$ fits better at larger evaporation rates.

To analyse the effect of different drop sizes, the radius of drop-2 was varied and the non-dimensional vapour fluxes along the surface of the two drops are plotted in Figure 9. *The physical parameters that define the vapour mass flux are ρ, D_{10}, R_0. A simple dimensional analysis shows that the vapour flux must be proportional to $\frac{\rho D_{10}}{R_0}$, which means that smaller drops have always a larger local vapour flux, while the evaporation rate (which is proportional to $n_v R_0^2$) must be larger.* Instead, the increase of the vapour flux on drop-1 is due to the reduction of the screening effect when the size of drop-2 decreases.

The distribution of the heat fluxes follows that of the vapour fluxes, since, as above pointed out, the two fluxes are proportional (see Eq. 44). A non-dimensional form of the heat flux can be defined by dividing the heat flux by that of an isolated drop of the same size, obtaining:

$$q_{ad,(b)} = \frac{q_{(b)}}{q_{is}} = n^{(1)}_{ad,(b)}$$

For the sake of comparison, the heat flux calculated assuming a constant density is non-dimensionalised in the same way, yielding:

$$q^c_{ad,(b)} = \frac{q^c_{(b)}}{q_{is}} = \frac{e^{M_0^c}\left(1 - e^{M_0}\right)}{e^{M_0}\left(1 - e^{M_0^c}\right)} n^c_{ad,(b)}$$

Thus, while the distribution of the non-dimensional heat flux evaluated by the present model is equal to that of the non-dimensional vapour flux, the same quantity evaluated assuming constant gas density differs from the corresponding vapour flux. Table 2 reports the value of the factor $\frac{e^{M_0^c}\left(1-e^{M_0}\right)}{e^{M_0}\left(1-e^{M_0^c}\right)}$ for the conditions of Table 1, $\delta = 1$ and $\beta = 2$.

Table 2. Values of the factor $\frac{e^{M_0^{(c)}}\left(1-e^{M_0}\right)}{e^{M_0}\left(1-e^{M_0^{(c)}}\right)}$ for the cases of Table 1.

Species	$T_\infty = 500$ K	$T_\infty = 750$ K	$T_\infty = 1000$ K
water	0.925	0.870	0.835
acetone	0.913	0.869	0.861
n-octane	0.945	0.920	0.961
n-dodecane	0.971	0.940	0.970

The factor $\frac{e^{M_0^c}\left(1-e^{M_0}\right)}{e^{M_0}\left(1-e^{M_0^c}\right)}$ is always lower than 1, while the ratio $\frac{M_0^c}{M_0}$ is always larger than 1 (see Figure 8). The constant density model predicts higher vapour fluxes and correspondingly lower heat fluxes, which is consistent to the fact that the presence of larger Stefan flows induces a reduction of the sensible heat fluxes.

4.2 The screening coefficient

The strength of the interaction between evaporating drops is usually characterised by the screening coefficient (also called *correction factor*, like in [22], or *reduction coefficient* like in [1], [5]) whose definition comes from a comparison with a single evaporating drop. In case of non identical drops, different screening coefficients can be defined, and the following ones are assumed thereinafter:

$$\phi_1 = \frac{m_{ev,1}}{m_{ev,is,1}};\ \phi_2 = \frac{m_{ev,2}}{m_{ev,is,2}}; \phi^T = \frac{m_{ev,1} + m_{ev,2}}{m_{ev,is,1} + m_{ev,is,2}} \tag{50}$$

where $m_{ev,is,b}$ is the corresponding evaporation rate of the isolated drop.

The coefficients ϕ_1 and ϕ_2 define the screening effect on each drop separately, while ϕ^T just compares the total evaporation rate from the two drops with that from the two drops at infinite distance (isolated).

A thermal screening coefficient can be defined as the ratio between the actual heat rate exchanged by a drop and that exchanged when the drops are at infinite distance ($Q_{is,(b)}$):

$$\phi_{th,(b)} = \frac{Q_{(b)}}{Q_{is,(b)}} \tag{51}$$

Due to the proportionality between heat and evaporation rates, the thermal screening coefficients are equal to the

evaporation screening coefficients. This result, that holds only for the case of drop evaporating into quiescent gas, was experimentally observed also for drops evaporating under convective conditions [5].

Figure 10(a) shows the effect of distance between the two non-identical evaporating drops on the screening coefficients. As it may be expected, the effect is larger for the smaller drop (the screening coefficients are always larger) and the difference between the two drops become larger as the drop radii ratio δ becomes smaller.

It is worth to notice that, applying the same definitions to the case of constant density, the resulting values of ϕ_j remain the same, since the constants M_0 and $M_0^{(c)}$, respectively for variable and constant gas density, drop out and then the screening coefficients only depend on geometrical configuration. This was already pointed out in [16]. Therefore, the present results about the screening coefficient are exactly comparable to those reported by [24].

For the case of identical drops, the three coefficients become equal and, using equation (30), an explicit function of the distance parameter β can be found:

$$\phi(\beta) = \sqrt{\beta^2 - 1} \sum_{p=0}^{\infty} \frac{2}{\left(\beta + \sqrt{\beta^2 - 1}\right)^{2p+1} + 1} \tag{52}$$

Figure 10(b) compares the values of the screening coefficient (Eq. 52) with the experimental results reported in [5] relative to the effect of drop neighbouring on the non-dimensional heat and mass transfer numbers (equivalent to the screening coefficient ϕ) for different liquids (ethanol, iso-hexane, n-decane, n-dodecane drops) and operating conditions.

As expected, the model under-predicts the screening effect (the theoretical curve is always higher than the experimental measurements), particularly for lower drop distances. Among the possible reasons for this discrepancy, the most relevant may be the following.

The model only considers a drop screened by the neighbouring one, while for the drop array each drop is directly screened by the two aside but also, in a weaker way, by all the others on the line. Thus the results of models based on two drop configuration can only be taken as upper limit for the screening coefficient. Moreover, the present model neglects the convective effects (only the Stefan flow is taken into account), which in drop-chain experiments are certainly important. Finally, since heat and mass fluxes are found to be non-uniform along the drop surface, a non-uniformity of drop temperature may be expected, and it has been shown that this influences the total heat and evaporation rates [39], with a clear possible effect on the screening coefficient.

5 Conclusions

The paper reports an analytical solution of the conservation equations to model the heating and evaporation of non identical drop pairs evaporating in quiescent gaseous environment, accounting for the dependence of the gaseous mixture density on temperature and composition. The solution in bi-spherical coordinate system allows to quantify the effect of drop neighbouring on heating and evaporation for any value of the Lewis number. Analytical forms of heat and vapour fluxes along the drop surface allow to estimate the detailed effect of drop interaction.

Comparison with the existing constant density model, for different species and operating conditions, shows that the classical approach yields larger values of the vapour flux and lower values of the heat flux. The differences are larger for higher gas temperature and become less evident for low volatile species.

Relative drop size affects the drop screening both on the overall heat and mass transfer and local fluxes. The decrease of one of the drop size causes the increase of the vapour fluxes of both drops. The vapour flux of the smallest drop increases due to the usual scaling effect, while the flux of the largest one increases due to the reduction of the screening effect.

The thermal and evaporation screening coefficients coincide and they are independent of the model assumption (constant or variable gas density).

References

[1] Sazhin, S., Droplets and Sprays, Springer, Heidelberg, 2014.

[2] Sazhin, S.S., Modelling of fuel droplet heating and evaporation: recent results and unsolved problems. Fuel, 196 (2017) 69-101.

[3] Zhifu, Z., Guoxiang, W., Bin, C., Liejin, G., Yueshe, W., Evaluation of evaporation models for single moving droplet with a high evaporation rate, Powder Technology, 240 (2013) 95-102.

[4] Abramzon, B., Sirignano, W.A., Droplet vaporization model for spray combustion calculations, International Journal of Heat and Mass Transfer, 32(9) (1989) 1605-1618.

[5] Castanet, G., Perrin, L., Caballina, O., Lemoine, F., Evaporation of closely spaced interacting droplets arranged in a single row, International Journal of Heat and Mass Transfer, 93 (2016) 788-802.

[6] Sangiovanni, J.J., Kesten, A.S., Effect of droplet interaction on ignition in monodispersed droplet streams, Proceedings of the Sixteenth International Symposium on Combustion (1976) 577-92.

[7] Sangiovanni, J.J., Labowski, M., Burning times of linear fuel droplet arrays: a comparison of experiment and theory, Combustion and Flame, 47 (1982) 15-30.

[8] Virepinte, J.F., Biscos, Y., Lavergne, G., Magre, P., Collin, G., A rectilinear droplet stream in combustion: droplet and gas phase properties, Combustion Science and Technology, 150 (2000) 143-159.

[9] Castanet, G., Lebouché, M., Lemoine, F., Heat and mass transfer of combusting monodisperse droplets in a linear stream, International Journal of Heat and Mass Transfer, 48 (2005) 3261-3275.

[10] Atthasit, A., Doué, N., Biscos, Y., Lavergne, G., Influence of droplet concentration on the dynamics and evaporation of a monodisperse stream of droplets in evaporation regime, Proceedings of the First International Symposium on Combustion and Atmospheric Pollution, Russia, July 8-11 (2003).

[11] Castanet, G., Maqua, C., Orain, M., Grisch, F., Lemoine, F., Investigation of heat and mass transfer between the two phases of an evaporating droplet stream using laser-induced fluorescence technique: comparison with modelling, International Journal of Heat and Mass Transfer, 50 (2007) 3670-3683.

[12] Deprédurand, V., Maqua, C., Castanet, G., Lemoine, F., Temperature measurement of evaporating ethanol/3-pentanone bicomponent droplets using 2-colour LIF, Proceedings of the 21st Conference on Liquid Atomization and Spray Systems, 10-12 September 2007.

[13] Deprédurand, V., Castanet, G., Lemoine, F., Heat and mass transfer in evaporating droplets in interaction: influence of the fuel, International Journal of Heat and Mass Transfer, 53 (2010) 3495-3502.

[14] Chiang, C., Sirignano, W.A., Interacting, convecting, vaporizing fuel droplets with variable properties , International Journal of Heat and Mass Transfer, 36(4) (1993) 875-886.

[15] Chiang, C. Sirignano, W.A., Axisymmetric calculation of three-droplet interactions, Atomization Sprays, 3 (1993) 91-107.

[16] Sirignano, W.A., Advances in droplet array combustion theory and modeling, Progress in Energy and Combustion Science, 42 (2014) 54-86.

[17] Dwyer, H.A., Stapf, P., Maly, R.R., Unsteady vaporization and ignition of a three dimensional droplet array, Combustion and Flame, 121 (2000) 181-94.

[18] Imaoka, R.T., Sirignano, W.A.,Transient vaporization and burning in dense droplet arrays , International Journal of Heat and Mass Transfer, 48 (2005) 4354–4366.

[19] Castanet, G., Frackowiak, B., Tropea, C., Lemoine, F., Heat convection within evaporating droplets in strong aerodynamic interactions, International Journal of Heat and Mass Transfer, 54(1516) (2011) 3267–3276.

[20] Frackowiak, B., Lavergne, G., Tropea, C., Strzelecki, A., Numerical analysis of the interactions between evaporating droplets in a monodisperse stream, International Journal of Heat and Mass Transfer, 53 (2010) 1392–1401.

[21] Brzustowski, T.A., Twardus, E.M., Wojcicki, S., Sobiesiak, A., Interaction of two burning fuel droplets of arbitrary size, AIAA Journal, 17 (1979) 1234-42.

[22] Labowsky, M., Calculation of the burning rates of interacting fuel droplets, Combustion Science and Technology, 22 (1980) 217-226.

[23] Umemura, A., Ogawa, S., Oshima, N., Analysis of the interaction between two burning droplets, Combustion and Flame, 41 (1981) 45 - 55.

[24] Umemura, A., Ogawa, S., Oshima, N., Analysis of the interaction between two burning fuel droplets with different sizes, Combustion and Flame, 43 (1981) 111-119.

[25] Marberry, M., Ray, A.K., Leung, K., Effect of multiple particle interactions on burning droplets, Combustion and Flame, 57 (1984) 237-245.

[26] Elperin, T., Krasovitov, B., Analysis of evaporation and combustion of random clusters of droplets or particles by the modified method of irriducible multipole expansion, Atomization Sprays, 4 (1994) 79-97.

[27] Imaoka, R.T., Sirignano, W.A., A generalized analysis for liquid fuel vaporization and burning, International Journal of Heat and Mass Transfer, 48 (2005) 4342 - 4353.

[28] Sirignano, W.A., Liquid-fuel burning with non-unitary Lewis number, Combustion and Flame, 148 (2007) 177-186.

[29] Fuchs, N.A., Vaporisation and droplet growth in gaseous media, Pergamon Press, London, 1959.

[30] Tonini, S., Cossali, G.E., On molar- and mass-based approaches to single component drop evaporation modelling, International Communications in Heat and Mass Transfer, 77 (2016) 87-93.

[31] Zubkov,V.S., Cossali, G.E., Tonini, S., Rybdylova, O., Crua, C., Heikal, M., Sazhin, S.S., Mathematical modelling of heating and evaporation of a spheroidal droplet, International Journal of Heat and Mass Transfer, 108 (2017) 2181-2190.

[32] R. Bird, W. Stewart, E. Lightfoot, Transport Phenomena, second ed., John Wiley and Sons, 2002.

[33] Slattery, J.C., Momentum, Energy and Mass Transfer in Continua, 2nd-edition, R. Krieger Publ. New York, 1981.

[34] Tonini, S., Cossali, G.E., An analytical model of liquid drop evaporation in gaseous environment, International Journal of Thermal Sciences, 57 (2012) 45-53.

[35] Yuen, M.C., Chen, L.W., On drag of evaporating droplets, Combustion Science Technology, 14 (1976) 147-154.

[36] Tonini, S., Cossali, G.E., A novel vaporisation model for a single-component drop in high temperature air streams, International Journal of Thermal Sciences, 75 (2014) 194-203.

[37] Moon, P., Spencer, D.E., Field Theory Handbook, Springer-Verlag, Heidelberg, 1988.

[38] Olver, F.W.J., Lozier, D.W., Bisvert, R.F., Clark, C.W. (Eds.) NIST handbook of mathematicalk functions, Cambridge University Press, 2010.

[39] Tonini, S., Cossali, G.E., Modelling of heat and mass transfer from spheroidal drops with non-uniform surface temperature, International Journal of Heat and Mass Transfer, 121 (2018) 747-758.

6 Figures

Figure 1. Sketch of the two-drop configuration.

Figure 2. Bi-spherical coordinate system.

Figure 3. Vapour molar fraction distribution, in terms of $H = \ln\left(1 - y^{(1)}\right)$, around (a) two identical drops and (b) two drops with size ratio δ= 0.5. Water, T_s=331.6K, T_∞=750K, $R_{d,1}$=20μm, β =2. Upper half: distribution for the variable density model (Eq. 27); lower half: distribution for the constant density model (Eq. 31).

Figure 4. Effect of gas and drop temperatures on the axial profile of $H = \ln\left(1 - y^{(1)}\right)$, with two identical drops for (a) water, (b) acetone, (c) n-octane and (d) n-dodecane. Solid and dashed lines refer to variable and constant density models, respectively. $R_{d,1} = R_{d,2}$=20μm, β =2.

Figure 5. Effect of gas and drop temperatures on the radial profile of $H = \ln\left(1 - y^{(1)}\right)$, with two identical drops for (a) water, (b) acetone, (c) n-octane and (d) n-dodecane. Solid and dashed lines refer to variable and constant density models, respectively. $R_{d,1} = R_{d,2}$=20μm, β =2.

Figure 6. Effect of drop distance (a) on the surface non-dimensional vapour mass flux and (b) on the deviation of the surface non-dimensional vapour mass flux from the maximum value, for water twin drops. Black and gray scatter-lines refer to variable and constant density models, respectively. $T_s = 331.6K, T_\infty = 750K$.

Figure 7. Effect of non-dimensional drop temperature on the ratio $\frac{M_0^c}{M_0}$ for different values of M_0^c and for all the operating conditions of table 1.

Figure 8. Effect of liquid species on the surface non-dimensional vapour mass flux, for twin drops for all the operating conditions of table 1, (a) $T_\infty = 500K$, (b) $T_\infty = 750K$, (c) $T_\infty = 1000K$. Black and gray scatter-lines refer to variable and constant density models, respectively. β=2.

Figure 9. Effect of drop size on the surface non-dimensional vapour mass fluxes for the two drops, β=2.

Figure 10. (a) Screening coefficients ϕ_1 and ϕ_2 as function of the distance parameter β for non-identical drop pairs and for different values of the drop radii ratio δ. (b) Screening coefficient as function of distance parameter (β) for an array of drops, as measured by [5] (symbols) and as predicted by the model (dashed line).

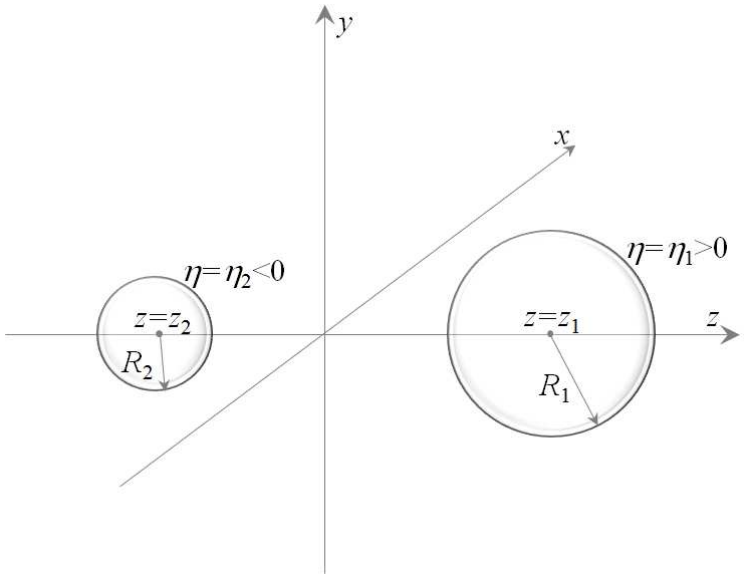

Figure 1. Sketch of the two-drop configuration. DISEGNARE teta

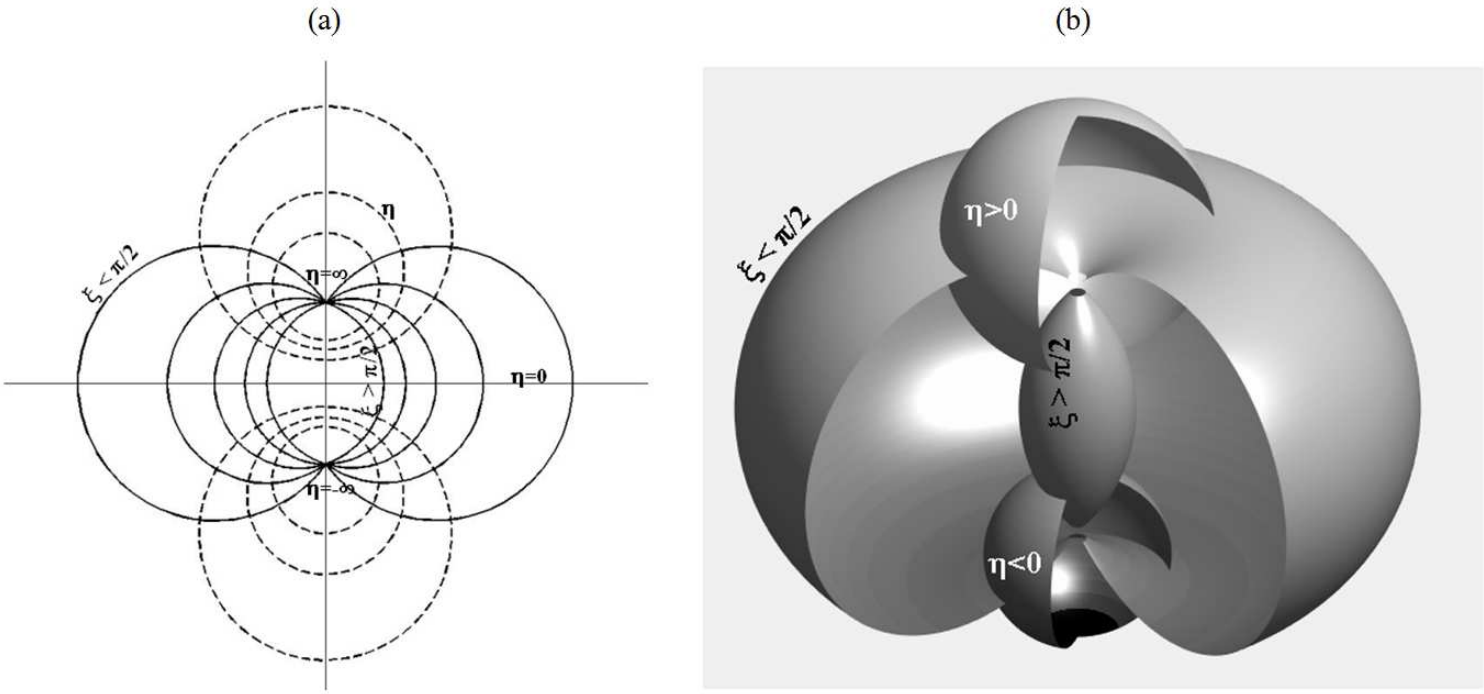

Figure 2. Bi-spherical coordinate system.

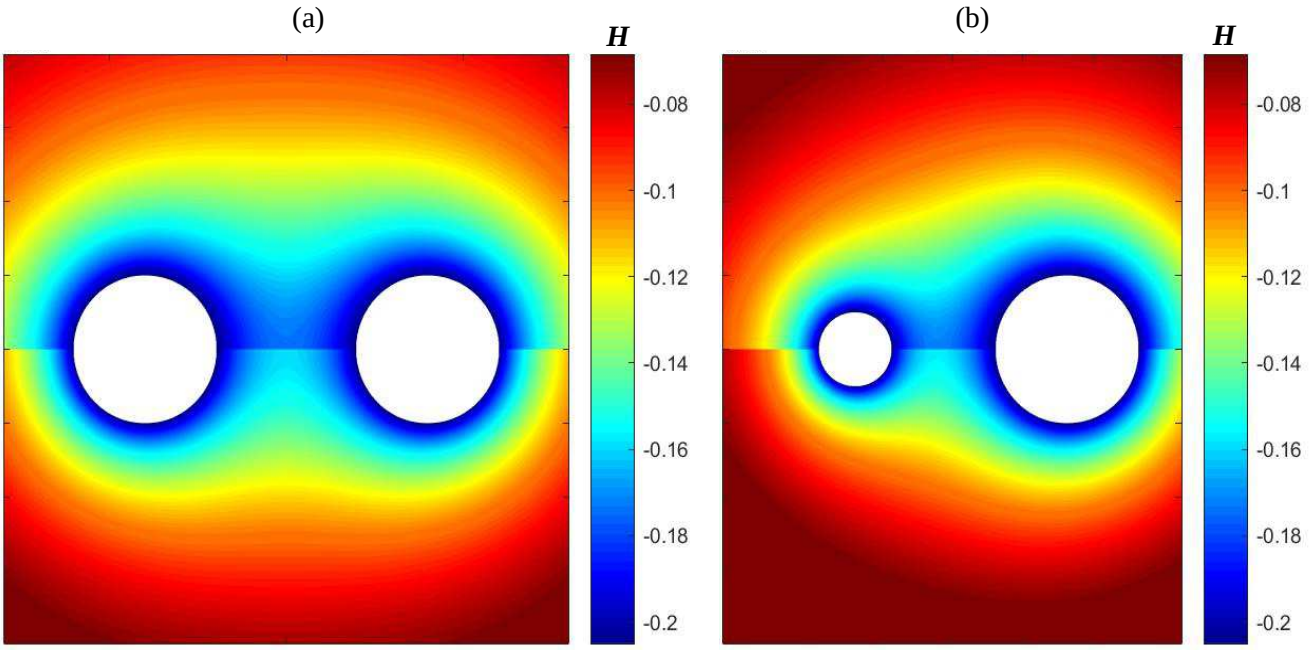

Figure 3. Vapour molar fraction distribution, in terms of H=ln(1-$y^{(1)}$), around (a) two identical drops and (b) two drops with size ratio δ= 0.5, $R_{d,1}$=20μm. Water, T_s=331.6K, T_∞=750K, β=2. Upper half: distribution for the variable density model (Eq. 26); lower half: distribution for the constant density model (Eq. 30).

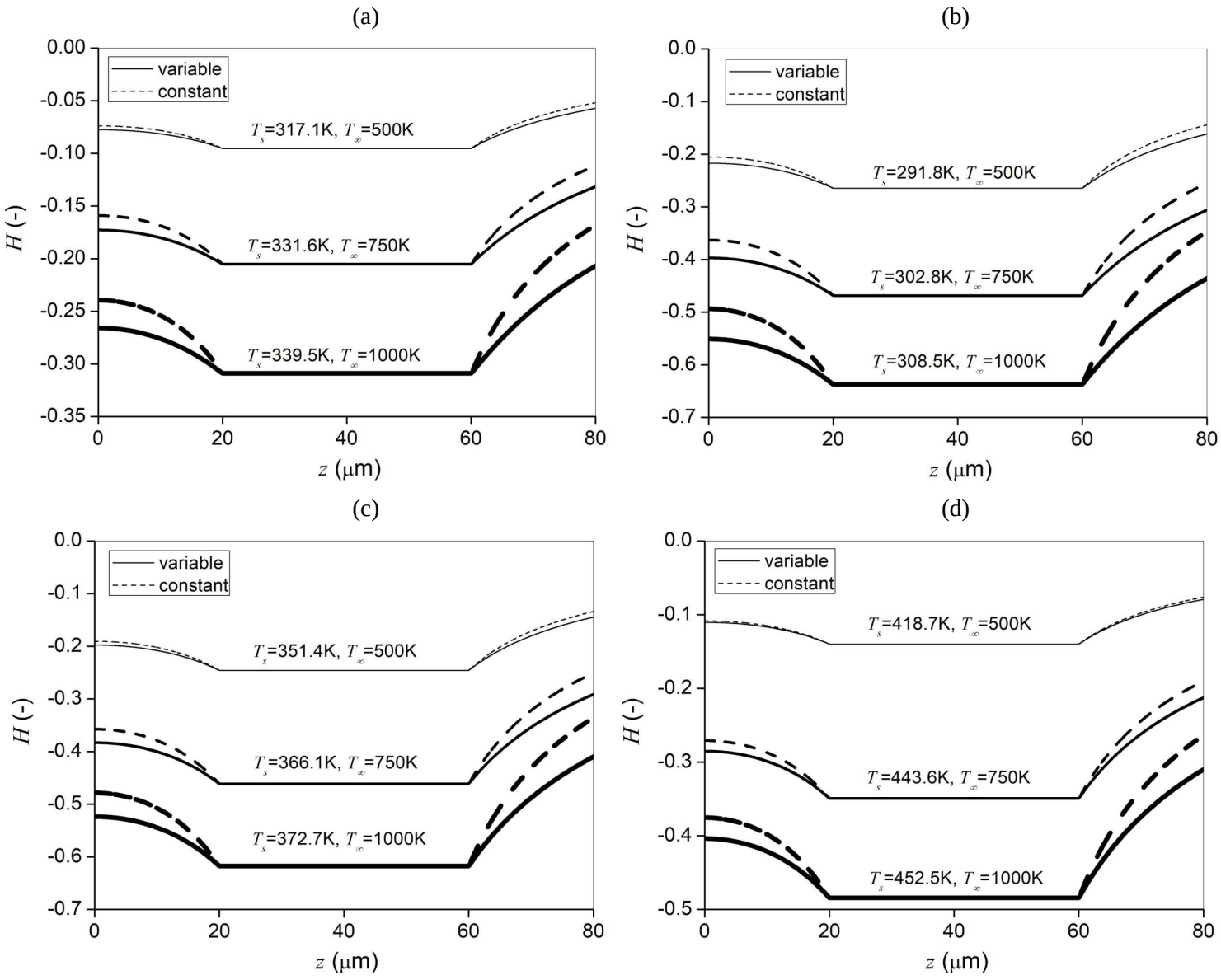

Figure 4. Effect of gas and drop temperatures on the axial profile of H=ln(1-$y^{(1)}$), with two identical drops for (a) water, (b) acetone, (c) n-octane and (d) n-dodecane. Solid and dashed lines refer to variable and constant density models, respectively. $R_{d,1}$=$R_{d,2}$=20μm, β=2.

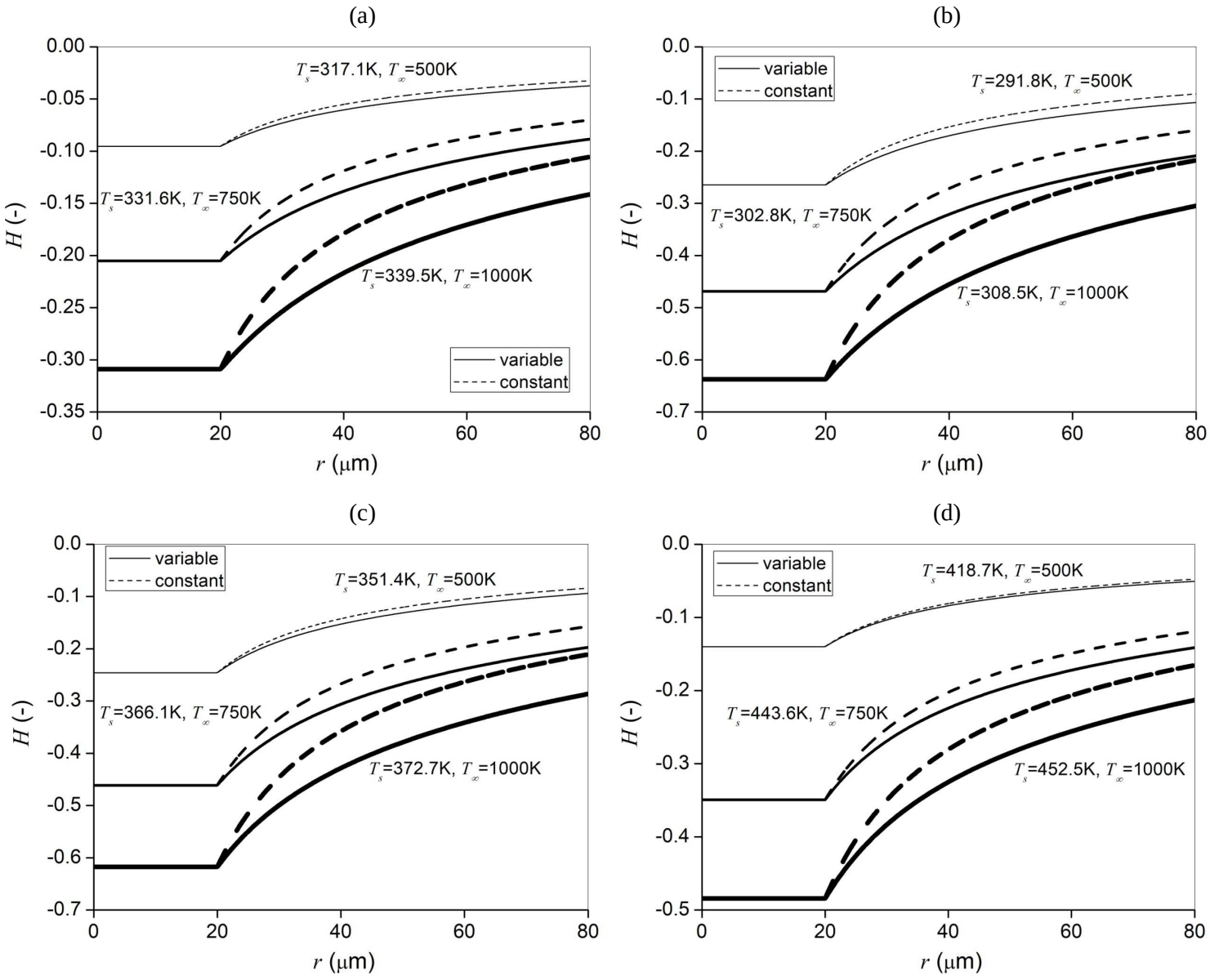

Figure 5. Effect of gas and drop temperatures on the radial profile of H=ln(1-$y^{(1)}$), with two identical drops for (a) water, (b) acetone, (c) n-octane and (d) n-dodecane. Solid and dashed lines refer to variable and constant density models, respectively. $R_{d,1}$=$R_{d,2}$=20μm, β=2.

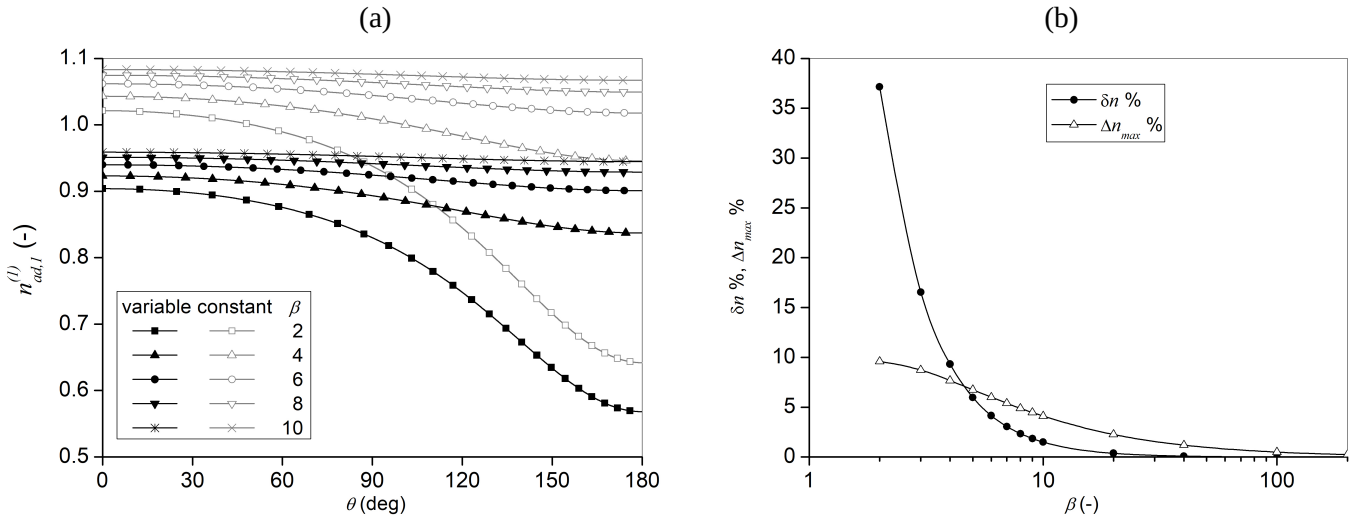

Figure 6. Effect of drop distance (a) on the surface non-dimensional vapour mass flux and (b) on the deviation of the surface non-dimensional vapour mass flux from the maximum value, for water twin drops. Black and gray scatter-lines refer to variable and constant density models, respectively. T_s=331.6K, T_∞=750K.

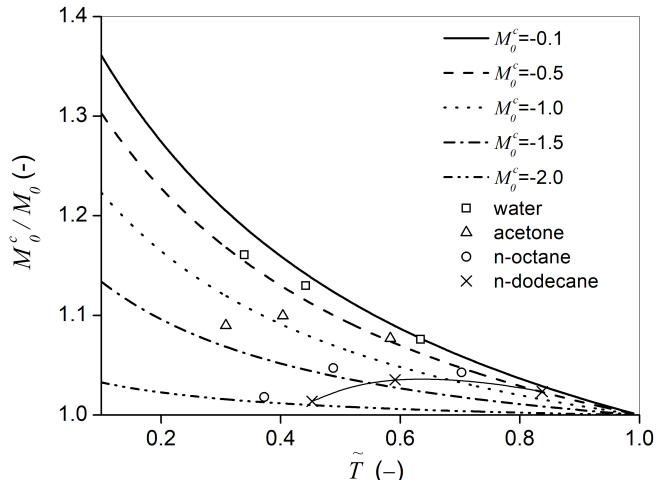

Figure 7. Effect of non-dimensional drop temperature on the ratio $\frac{M_0^c}{M_0}$ for different values of M_0^c and for all the operating conditions of table 1.

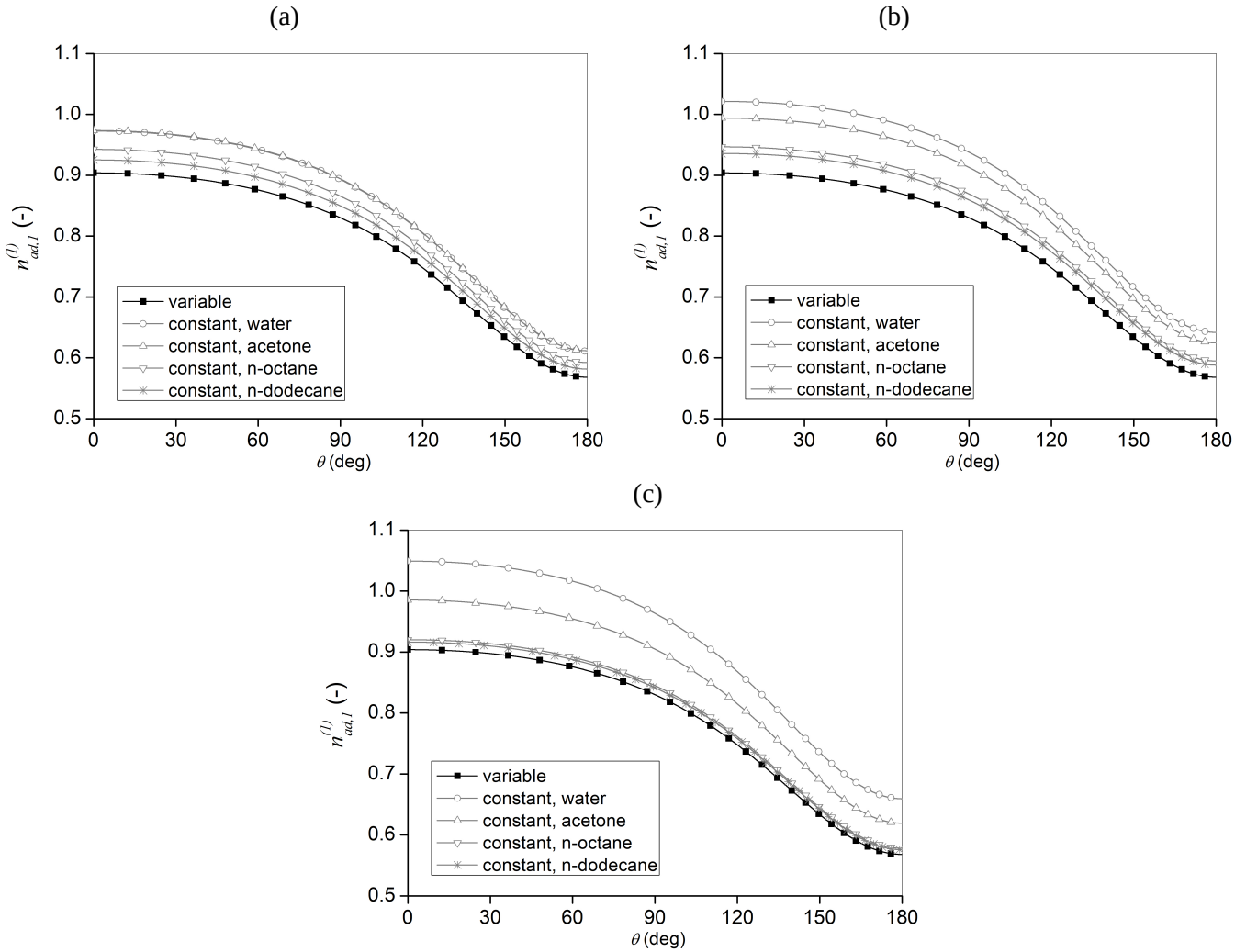

Figure 8. Effect of liquid species on the surface non-dimensional vapour mass flux, for twin drops for all the operating conditions of table 1, (a) T_∞=500K, (b) T_∞=750K, (c) T_∞=1000K. Black and gray scatter-lines refer to variable and constant density models, respectively. β=2.

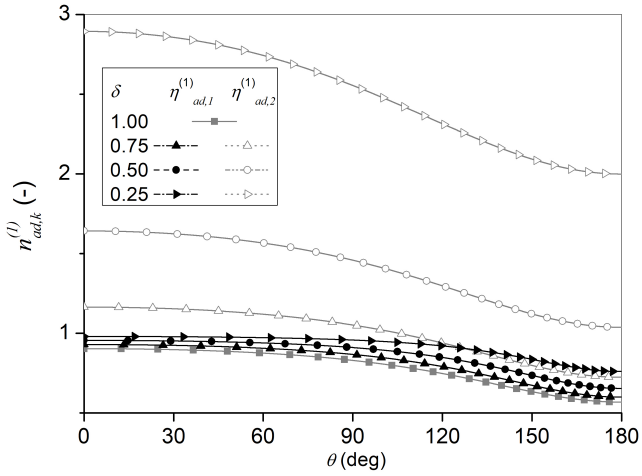

Figure 9. Effect of drop size on the surface non-dimensional vapour mass fluxes for the two drops, β=2.

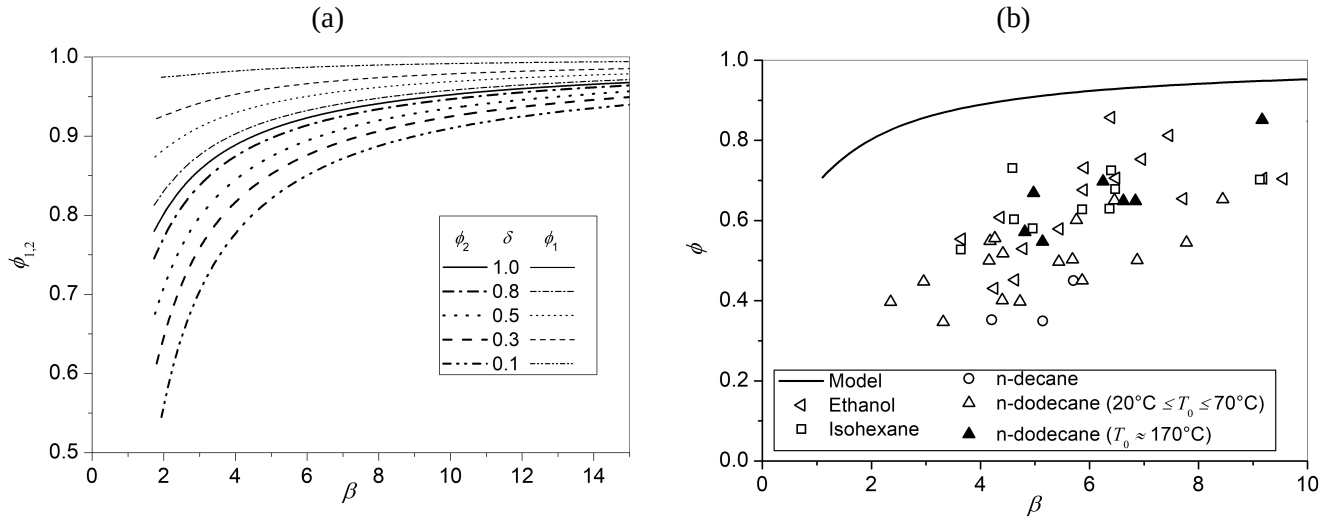

Figure 10. (a) Screening coefficients ϕ_1 and ϕ_2 as function of the distance parameter β for non-identical drop pairs and for different values of the drop radii ratio δ. (b) Screening coefficient vs distance parameter (β) for an array of drops, as measured by <cite>Castanet2016</cite> (symbols) and as predicted by the model (solid line).